Divergence in a stress-associated gene regulatory network underlies differential

2 growth control in the Brassicaceae family

- 4 Authors: Ying Sun^{1*}, Dong-Ha Oh^{2*}, Lina Duan¹, Prashanth Ramachandran¹, Andrea
- 5 Ramirez¹, Anna Bartlett³, Maheshi Dassanayake², José R Dinneny^{1#}

Affiliations

- 7 1 Department of Biology, Stanford University, 371 Jane Stanford Way, Stanford, CA 94305,
- 8 USA

1

3

6

13

14

- 9 2 Department of Biological Sciences, Louisiana State University, Baton Rouge, LA, 70803, USA
- 10 3 Genomic Analysis Laboratory, Salk Institute for Biological Studies, La Jolla, CA, USA
- 11 * These authors contributed equally to this work.
- 12 Correspondence should be addressed to dinneny@stanford.edu.

Abstract

- 15 The use of marginal lands in agriculture is increasingly necessary to support the global
- human population. Elevated salinity frequently occurs in degraded soils and hinders
- their use due to the negative impact salt stress has on plant growth. While the hormonal
- 18 networks controlling growth have been extensively characterized in stress-sensitive
- plants, it is unclear how these pathways are rewired in plants that maintain growth in
- 20 extreme environments. We have compared the physiological and molecular responses
- of four closely related members of the Brassicaceae family including two salt-tolerant
- 22 species (Shrenkiella parvula and Eutrema salsugineum) and two salt-sensitive species
- 23 (Sisymbrium irio and Arabidopsis thaliana) to the salt stress-induced hormone, abscisic
- 24 acid (ABA). While ABA inhibits root growth in most species, we uncovered substantial
- 25 growth-promoting effects in *Shrenkiella parvula*, due to an enhancement in cell
- 26 elongation. Comparative transcriptomics informed by phylogenetic relationships
- 27 uncovered lineage and extremophile-specific differences in ABA response. DNA Affinity
- 28 Purification followed by sequencing (DAP-Seq) was utilized to establish gene regulatory
- 29 networks (GRNs) in each species for the entire ABA-RESPONSIVE ELEMENT
- 30 BINDING FACTORS (AREB/ABF) clade. Comparative GRN analysis identified relative
- 31 conservation in the core ABA signaling GRN, while the auxin growth-hormone GRN was
- 32 highly divergent, revealing how patterns of gain and loss of cis-regulatory elements
- 33 mediate novel physiological outcomes. Our findings demonstrate that the targets of
- 34 hormone signaling pathways are highly divergent between species and that diametric
- inversion of growth regulation is possible, even between closely related species of the
- 36 same plant family.

Keywords: abscisic acid, extremophile, AREB/ABF, DAP-Seq, halophyte, Brassicaceae

Introduction

The survival of all organisms depends on their ability to appropriately respond to environmental signals, which is superbly exemplified by plants, whose physiology and growth is constantly tuned to suit the context ¹. During periods of environmental stress, some plants are better able to cope than others ². The most widely characterized plants are typically stress-sensitive, such as the molecular-genetic model *Arabidopsis thaliana* (At) and domesticated crops. Our limited knowledge of the most effective response strategies to stress currently limits our ability to maintain agricultural yields in the face of global climate change ³.

Extremophytes (stress-tolerant plants) are plant species that have evolved mechanisms to cope with various abiotic stresses such as cold, drought, and hypersaline conditions ⁴ ⁵. Recently, the reduced cost of sequencing has provided new opportunities to study the genes that underlie these physiological adaptations to extreme environments (**Fig. 1b**) ⁶ ⁷. Within the Brassicaceae, two halophyte plant species exhibit greater tolerance to soil salinity than the model plant At. *Eutrema salsugineum* (Es) is tolerant to the effects of salt and grows along the ocean shorelines of Shandong province in China, while *Schreinkiella parvula* (Sp) grows near Lake Tuz in Turkey, and is tolerant to high levels of Na⁺, Li⁺, Mg²⁺, and Boron ^{8 9}. While At belongs to Lineage I of the Brassicaceae family, both extremophytes belong to lineage II, which also contains the stress-sensitive species *Sisymbrium irio* (Si)¹⁰. These species, being diploid, with small genomes, and similar numbers of genes, present new opportunities to understand how stressmediated gene networks in extremophytes differ from stress-sensitive plants ¹¹ ¹².

While salt tolerance in Es has been previously associated with strategies that maintain growth including effective energy use, regulation of excess electron flow, protective barriers in the root, and chloroplast protection, salt tolerance in Sp is less well understood ^{13 14}. Many environmental stressors lead to the synthesis and activation of the abscisic acid (ABA) plant hormone signaling pathway. In At, ABA inhibits germination, root growth, and gas exchange as a means of limiting growth under abiotic stress and preserving resources ^{15 16 17}.

ABA perception triggers a signaling cascade that leads to the phosphorylation of bZIP transcription factors (TFs) known as ABA-RESPONSIVE ELEMENT BINDING FACTORS (AREB/ABFs) ¹⁸ ¹⁹. ABFs relocalize to the nucleus and activate gene expression by binding to cis-regulatory elements (CREs) known as *ABA-RESPONSIVE ELEMENT*s (*ABRE*) (**Fig. 1a**). Thousands of genes, in various tissues, are activated upon ABA treatment to confer its physiological effects in At. We hypothesized that

defining how the architecture of the ABA-mediated gene network varies across species will elucidate whether environmental-response programs become tuned to extreme environments over evolutionary timescales ²⁰.

In this study, we examined the sensitivities of the extremophytes to exogenous ABA treatment and uncovered substantial differences, most notably in Sp. We conducted RNA-Seq to capture the transcriptional profile of both root and shoot tissue at short and long time points to identify genes and pathways that support plant growth during stress conditions. We also performed DAP-Seq to characterize the transcription factor binding landscape that mediates the physiological effects of ABA signaling. We applied a method we termed, swap-DAP to determine the contribution of cis- and trans-regulation on the transcription factor binding landscape defined by DAP-Seq. Finally, we combined these data into gene networks to define conserved and species-specific components of the ABRE/ABF-mediated gene regulatory network and identify genes and subnetworks that may be important for stress tolerance in extremophytes. Together, this work has revealed the patterns of variation that differentiate stress tolerant and sensitive species and identify specific rewiring events that allow Sp to maintain growth despite a stressful environment.

Results

77

78

79 80 81

82

83

84 85

86

87

88 89

90

91 92

93

94

- 96 A comparison of the growth response to ABA treatment reveals a diametric switch in the
- 97 behavior of Sp roots.
- 98 ABA mediates the regulation of root growth under salinity and drought. We
- 99 hypothesized that studying the effects of ABA on root growth would therefore be a
- useful approach for interrogating variation in stress response pathways and would avoid
- the challenge of comparing transcriptional programs between species using different
- stress treatment regimes. As was previously described, we found that At and Si root
- growth is dramatically inhibited under elevated concentrations of NaCl, while Sp and Es
- exhibit substantial tolerance to these effects (Fig. 1c). In contrast, the application of
- exogenous ABA revealed that these treatments had inhibitory effects on primary root
- growth in all species except Sp, which exhibited a striking promotion of growth at all
- 107 concentrations tested (**Fig. 1d**). We characterized the developmental basis for the
- observed growth enhancement (Fig. 1e) and found that while the meristem size for At
- and Sp is reduced upon ABA treatment (Fig. 1f), final cell length for Sp increased by
- 110 50% (from ~100 μm to ~200 μm) after treatment while no changes occurred in At (**Fig.**
- 111 **1g-h**). These data show that all species tested respond to ABA by differential growth.
- but that the direction of this effect can vary dramatically depending on the species and
- 113 developmental context.

114 Comparative transcriptomics informed by phylogenetic relationships uncovered lineage 115 and extremophyte-specific differences in ABA response 116 To more broadly establish how responses to ABA might vary, we performed RNA-Seq 117 on the roots and shoots of all 4 species, either treated with mock or 10 µM ABA, and 118 harvested tissues at 3 hours and 24 hours post-treatment. While we captured known 119 ABA response genes in At and observed the greatest number of genes differentially 120 expressed (DE) at 3 hours in the root for At, Si, and Es, Sp again stood out with an 121 almost equal number of DE genes in both 3 hours and 24 hours root samples, while the 122 greatest number of genes in Sp appear in the shoot at 24 hours (Fig. 2a). Upon 123 clustering DE genes in each species and ranking the clusters from greatest to the 124 fewest number of genes within each cluster, Sp again appears to exhibit striking 125 differences in cluster patterns (Fig. 2b). While we identified a subset of species-specific 126 genes, the greater proportion of genes have Arabidopsis orthologs which facilitates a 127 cross-species comparison of gene regulation (Fig. 2c, Supplementary Dataset 1). Using CLfinder, we defined 15,198 unambiguously 1-to-1 orthologous gene groups 128 129 across our four species (Supplementary Fig. 1, Supplementary Dataset 1,2). We 130 categorized ABA-responsive genes based on whether they showed broad conservation 131 or were regulated in a lineage, species, or extremophile-specific manner. In ranking 132 these categories, we found that conserved responses were the least prevalent while 133 stress-sensitive or extremophyte associated responses were the most prevalent (Fig. 134 2d). We identified patterns of GO category enrichment for DE genes (DEGs) on a per-135 species basis, contrasting ABA-induced and repressed DEGs. Among ABA-induced 136 DEGs, we found an extensive overrepresentation of "response to abiotic stimulus" and 137 10 related non-redundant GO terms in all samples and species (Supplementary Fig. 2, 138 Supplementary Dataset 3). These GO terms cumulatively accounted for 20 to 25% of ABA-induced DEGs in all samples and were not detected among ABA-repressed DEGs. 139 140 141

The phylogenetic relationship of species studied here provides an opportunity to systematically detect lineage-specific modifications in pathway regulation. To identify such patterns, we developed a phylogenetically informed profiling (PiP) approach that utilizes a correlation metric to establish whether pairs of species exhibit a similar regulatory program for genes associated with a particular Gene Ontology (GO) category (Supplementary Fig. 3a, Supplementary Dataset 4). The GO term "response to abscisic acid" showed significant correlations in all species pairs indicating broad conservation in the valence of gene regulation, likely inherited from the last common ancestor (Fig. 2e). In contrast, orthologous gene pairs associated with protein translation ("peptide biosynthetic process") exhibited no correlation, or showed anticorrelation, between Sp and other species in root tissues 3 hours post ABA treatment. This pattern suggests an Sp-specific change in regulation (Fig. 2f). Several GO terms related to ribosomal function and translation showed the largest variances of

142

143

144

145

146

147

148

149

150

151

152

- 154 Spearman correlation coefficient (ρ) among species pairs, especially in root samples,
- suggesting divergence in the responses of Sp orthologs to ABA (**Supplementary Fig.**
- 156 **3b**). Protein translation is finely orchestrated with the metabolic activity in cells and
- 157 corresponds to the growth cellular state ²¹. Our data suggest that Sp interprets ABA
- signaling as a proxy for environmental stimuli where growth is enhanced, rather than
- suppressed as it is in all other species examined here.
- To profile the factors that drive differential gene expression across species, we
- analyzed the promoters of highly ABA-responsive DEGs (fold-change ≥ 2) using
- 163 Analysis of Motif Enrichment (AME) (McLeay and Bailey 2010). In looking for over-
- represented TF binding motifs within 1 Kb of upstream DNA sequence of the promoter
- region, we found motifs for ABF1/2/3/4 and an additional 32 TFs, all of which included a
- 166 G-box like motif similar to the previously defined ABRE motif 22 (Supplementary Fig. 4,
- Supplementary Dataset 5). Interestingly, none of these motifs were found enriched in
- the promoters of ABA-repressed DEGs suggesting these motifs are associated with
- transcriptional activators. Considering patterns of enrichment in gene functions and
- 170 known regulatory motifs, we hypothesized that ABA primarily acts first on the up-
- 171 regulation of gene expression through binding of ABFs, while the signal diversifies
- through ABF GRNs to create more intricate responses depending on the tissue and
- temporal contexts.

160

- 174 The gain and loss of ABREs at the nucleotide level led to differences in the binding
- 175 landscape of ABFs
- 176 To understand the molecular mechanism underlying the divergence in ABA-induced
- transcriptional changes across species, we sought to establish global maps of ABF
- binding in Sp. Si, Es, and At. The recent development of DNA affinity purification (DAP-
- 179 Seg) provided a method amendable for the study of non-model organisms. In contrast
- with ChIP-Seg, DAP-Seg facilitates the direct measurement of TF to genomic DNA
- 181 (gDNA) binding without the need to develop TF-specific antibodies or generate
- transgenic lines with epitope-tagged TFs ²³. Fortuitously, ABFs have 4 homologs within
- each of our model species and 4 paralogs across each species (Supplementary Fig.
- 184 **5**). Therefore 16 ABFs were characterized for their ability to bind to the At genome as
- well as the genomes of Es, Si, and Sp. A minimum of 2 biological replicates were used
- 186 for each pull-down and purified genomic DNA from shoot tissue was used in all cases
- due to the low-quality of data obtained using root-derived gDNA. Stringent criteria were
- established to ensure a high level of quality amongst the processed samples.
- 189 (Supplementary Fig. 6).

- 191 To determine if the DNA-binding affinity of ABFs varies across isoforms, we performed
- motif analysis on the genomic regions bound by ABF using GEM ²⁴. Highly similar

ABRE-like motifs were identified as the most predominant binding site indicating that DAP-Seq is able to uncover the genome-wide binding landscape of ABFs across related Brassicaceae species (**Fig. 3a**). To determine the specificity of the DAP-Seq assay, we compared the proportion of ABREs occupied by DAP-Seq peaks to the distribution of the core sequence (ACGT) that centers the ABRE motif across the genome and found that ABREs as well as ABF binding occurs in higher proportion in the 5' promoter region upstream of genes compared to the ACGT sequence, which does not have a feature preference (**Supplementary Fig. 7, Supplementary Dataset 6**).

193194

195

196

197198

199

200

201202

203

204

205

206

207

208

209

210

211212

213

214

215

216

217

218

219

220

221

222

223

224225

226

227

228

229

230

231

232

To further profile differences and similarities in the binding landscape, we compared the binding positions of the top 3000 ABF binding sites. We found significant overlap for ABFs within each species, indicating that the ABFs function redundantly to regulate downstream gene expression. To investigate the role of cis or trans effects, we swapped the cognate genome for a noncognat genome (*Arabidopsis*) during the pull-down which we termed swap-DAP. The large overlap of binding positions across species suggest that the cis-effect from the genome, instead of the TF isoform used, contributes the greatest difference in ABF binding landscape (**Fig. 3b, Supplementary Fig. 8**).

We assigned significant TF-DNA associations based on the proximity of the binding site to the nearest gene. This analysis identified 14,374 ABF-target associations for At and 10,558 for Si, 10,197 for Sp, and 20,026 for Es. These data are of particular significance as no prior information on TF-DNA interactions were available for Si, Sp, and Es. While we identified large overlaps in ABF function within species, we hypothesize that differences in ABF binding across species may rewire transcriptional responses and potentially repurpose gene networks to confer different responses to ABA. Leveraging the strength of our cross-species datasets, we characterized incidences where the ABF binding profile is altered in Sp compared to other species. For example, in AT2G21510, all ABF1/2/3/4 bind to the 5' proximal region of this gene, which is annotated as a molecular chaperone important for tolerating environmental stress. This is also true for AT5G42570, which is annotated as B-cell receptor-associated 31-like protein, previously found to be associated with cold acclimation ²⁵. However, while At, Si, and Es show ABF binding, Sp does not. Changes in binding profile are associated with differences in gene expression, where both AT2G21510 and AT5G42570 have greater transcript abundance under 10 µM ABA treatment in most species while the Sp orthologues have greater transcript abundance under control conditions. Our swap-Dap data set suggest that these changes are due to cis-effects since Sp ABF isoforms are able to bind these promoter regions in the At genome (Fig 3c, Supplementary Fig. 9). Alignment of the promoter regions across species revealed that, in the two genes highlighted from our analysis, the core ABRE motif is disrupted in Sp due to a single

base pair mutation. Interestingly, the promoters of AT2G21510 and AT5G42570 have several other ABRE-like sequences that underlie the DAP-seq peak and are fully conserved in Sp (**Fig 3d, Supplementary Fig. 10**). These other ABREs may not be sufficient to recruit ABFs due to differences in flanking sequence or higher order

237 structural features of the locus. Thus, our analysis highlights how DAP-Seq can be used

to profile functional binding site motifs and identify motif-disrupting variants that alter TF

binding and target gene expression.

To test more broadly how well-correlated ABF binding is to ABA-regulated gene

- expression, we tested whether genes including a DAP-seq peak in adjacent genomic
- 243 regions were enriched among ABA-induced and repressed DEGs. Among ABA-induced
- DEGs, the most significant enrichment was found for the presence of a DAP-seq peak
- in the 5' proximal 1Kb regions, followed by 5' distal 1Kb regions, while less to no
- significant enrichments were observed for a DAP-seq peak in the 3' region (Fig 3e).
- This pattern was not observed among ABA-repressed DEGs (**Supplementary Table 1**).
- Our method highlights the strength of comparative studies in identifying genetic variants
- with molecular functions which could leverage TF-binding landscapes as an emerging
- 250 phenotype that can be used to connect genetic variants with differences in growth
- 251 strategies.

238

239240

- 252 The gain and loss of ABF-binding has led to the rewiring of GRNs controlled by ABA
- 253 signaling

- We hypothesized that changes in the regulation of growth by ABA is modulated by
- changes in the architecture of the ABF gene regulatory network (GRN) between
- species. To test this, we explored rewiring patterns in Sp, compared to At, by first
- 257 stratifying the GRN into primary and secondary modules. We used the nodes and edges
- of the primary ABA network defined in Song et al. as a scaffold to map our DAP-Seq
- derived ABF edges on top ²⁶. We found that a majority (46/53) of the initial nodes of the
- 260 network were also predicted ABF targets in At. Among these 46 genes, we found only 3
- 261 that were no longer targets of ABFs in Sp (**Supplementary Fig. 11**). Supporting these
- observations, we found similar transcriptional responses of these genes when
- 263 comparing At and Sp, suggesting deep conservation of the ABF-mediated network.
- Since ABA crosstalks with other hormone pathways, we hypothesized that divergence
- in the ABA GRN might also occur beyond the primary network. We focused on auxin
- and ethylene pathways since previous literature has shown that they cross-talk with
- ABA in the context of growth control ²⁷ ²⁸ ²⁹. We curated a list of genes with roles in
- 269 biosynthesis, transport, and signaling pathways for auxin (199 genes) and ethylene (72
- 270 genes) 30 31 32 33 34 35 36 37 38 39 40(Supplementary Fig. 11, 12). From these datasets, we
- found that 33 ethylene and 81 auxin-related genes were targeted by ABFs in at least

one species (At or Sp). 18 out of 33 ethylene-related genes exhibited differences in ABF binding between At and Sp, however these changes were observed in other lineage II species as well. Among the differentially wired genes we found only 2 that are rewired in an Sp-specific manner. In contrast, we observed a larger proportion of auxin-related genes (15/81) with differences in ABF binding specifically in Sp compared to At. Additionally, we found an equal number of genes that displayed differential ABF binding in Sp and one of the other lineage II species. (**Fig. 4a**). Our transcriptome dataset is aligned with these findings and suggests a repurposing of an auxin related subnetwork since we observed many Sp orthologs displaying transcriptional patterns that could be explained by differences in ABF binding (**Fig. 4b**).

Auxin inhibits root growth by suppressing the rate of cell elongation ⁴¹. We observed that a large number of genes that encode enzymes involved in auxin biosynthesis are rewired in the Sp ABF network (Fig. 4a), including TAA1 and YUC2, which mediate the last steps of auxin biosynthesis. While these genes are induced by ABA in At, this effect is lost in Sp (Fig. 4b), suggesting that the divergence in growth regulation by ABA may, in part, be mediated by differential control of TAA1/YUC2. To validate this hypothesis, we utilized a TAA1 inhibitor, L-Kyruneine ⁴², to inhibit auxin biosynthesis. In At, L-Kyruneine reduced the sensitivity of roots to ABA treatment, consistent with previous work demonstrating the importance of auxin in mediating the response to ABA ⁴³. Similarly, the TAA1 loss of function allele wei8-1 44 exhibited resistance to ABA treatment (Fig. 4c). Together, these data suggest that ABA mediated growth inhibition depends on TAA1 and auxin biosynthesis (Fig. 4d). We hypothesize that in Sp, this growth inhibitory arm may be strongly diminished since the regulation of TAA1/YUC2 is no longer targeted by ABFs. Thus, the ultimate physiological outcome of ABA on primary root growth depends on the degree to which auxin biosynthesis and signaling are induced by ABF binding and transcriptional regulation.

Discussion

In our study, we aimed to investigate how stress-mediated gene networks differed between extremophytes and non-extremophile species to elucidate the components by which plants have altered ancestral networks to gain beneficial traits. We selected species in the Brassicaceae to take advantage of the extensive gene annotation and knowledge associated with *Arabidopsis*. Through transcriptional profiling and a phylogenetically informed bioinformatics approach, we were able to identify networks and pathways controlling growth with lineage-specific and species-specific differences. We found that ABFs play a large role in mediating ABA signaling since over 50% of the ABF binding sites were associated with differential expression.

Our study also highlights the first analysis conducted to explore the transcription factor binding landscape in Si, Sp, and Es as well as the use of the swap-DAP assay to distinguish between cis and trans contributions to the binding landscape. These datasets present a new resource for comparative analysis across Brassicaceae species and a model for comparative functional genomics. While our study focused on comparing 1 vs. 1 orthologs across species, these datasets can also be mined to characterize species-specific genes of unknown function and the consequence of gene duplication across species.

Using these methods, we observed several incidences where the gain or loss of ABREs near ABA-responsive genes led to differences in transcript abundance for that gene across species. This correlates with our hypothesis that the gain or loss of CREs is an important mechanism used by plants to rewire ancestral GRNs during the evolution of adaptive traits. Previous work has proven the utility of manipulating the promoter sequences of plant growth regulators to generate agriculturally beneficial traits in crops ⁴⁵. The work presented here has identified genes whose promoters have likely been the target of natural selection for extreme stress tolerance and will likely fuel the further implementation of a genetic engineering strategy for crop improvement that targets gene regulatory sequence. Future work to incorporate more Brassicaceae species into our comparative framework will better elucidate the genetic variants that define the specificity of GRNs especially in cell-type specific contexts.

ACKNOWLEDGEMENTS

We would like to acknowledge Mary Galli and Muh Ching Yee for advice on experimental design, Carnegie Institution for Science, Department of Plant Biology and Garret Huntress for providing access to computing resources and data management. Chris Pires for *S. irio* seeds. Funding was provided by the US Department of Energy's Biological and Environmental Research program (Grant DE-SC0020358, to J.R.D., D.H.O and M.D), the Carnegie Institution for Science endowment (J.R.D), National Science Foundation (MCB-1616827 and NSF-IOS-EDGE-1923589) and RDA, South Korea (Next-Generation BioGreen21 program PJ01317301) to DO and MD, and a National Science Foundation Graduate Research Fellowship (Y.S.). José Dinneny is also supported in this work as an HHMI-Simons Faculty Scholar.

AUTHOR CONTRIBUTIONS

- YS, DO, MD and JRD designed the research. YS and LD performed the experiments.
- YS, DO, PR, AR and JRD analyzed the data. YS and JRD wrote the manuscript. DO,
- LD, and PR contributed to the manuscript preparation.

SUPPLEMENTARY INFORMATION

List of Supplementary Text, Figures, Tables, and Datasets

- 355 Main figure 1: S. parvula responds differently to ABA.
- 356 Main figure 2: RNA-Seq identifies genes regulated by ABA across species.
- 357 Main figure 3: Differences in the transcriptional response are partially due to differences in the AREB/ABF
- 358 binding landscape across species.
- 359 Main figure 4: Rewiring of ABF-Auxin biosynthesis regulatory network is responsible for altered growth
- 360 response in S. parvula.

350 351

352 353

354

- 361 Supp. figure 1: Genome versions used in current study and detection of all 1-to-1 ortholog groups.
- 362 Supp. figure 2: Enrichment of Gene Ontology (GO) term "response to abiotic stimulus" and related GO
- 363 terms among ABA-induced Differently Expressed Genes (DEGs).
- 364 Supp. figure 3: Phylogenetically informed Profiling (PiP) analysis of ABA-responses.
- 365 Supp. figure 4: Transcription factor (TF)-binding motifs enriched among ABA-induced DEGs.
- 366 Supp. figure 5: AREB/ABFs of different species cluster together based on protein sequence and have
- 367 conserved DNA-binding and protein-protein interaction domains.
- 368 Supp. figure 6: Quality control checks to confirm the DAP-Seq assay works as expected.
- 369 Supp. figure 7: Distribution of ACGT and ABRE motifs and proportions occupied by a DAP-seg peak
- 370 Supp. figure 8: Ranks and overlap of DAP-seq peaks.
- 371 Supp. figure 9: ABF binding in AT5G42570 and orthologs across species is lost in S. parvula.
- 372 Supp. figure 10: Core ABRE is mutated in Sp ortholog of AT5G42570.
- 373 Supp. figure 11: Integration of ABF transcription factors into hormone (ABA and Ethylene) gene
- 374 regulatory networks in S. parvula.
- 375 Supp. figure 12: Comparison between A. thaliana and S. parvula data sets reveal changes in ABF
- 376 mediated Auxin gene regulatory network.
- 377 Supplementary Table 1: Dataset of ABA-responsive genes with DAP-seg peaks among up- and down-
- 378 DEGs
- 379 Supplementary Dataset 1: All 1-to-1 Orthologous group with functional genomics data from RNA-seq and
- 380 DAP-seq.
- 381 Supplementary Dataset 2: An analysis with OrthNet (including duplicates) with functional genomics data
- from RNA-seg and DAP-seg.
- 383 Supplementary Dataset 3: GO enrichment among ABA-induced and repressed DEGs.
- 384 Supplementary Dataset 4: Results from PiP analyses.
- 385 Supplementary Dataset 5: JASPAR motifs enriched among promoters of ABA-induced and repressed
- 386 DEGs

389 390

391

394

- 387 Supplementary Dataset 6: All DAP-seq peak coordinates with annotation (ACGT/ABRE and genomic
- regions), and rank.

CORRESPONDENCE

- 392 Correspondence and requests for materials should be addressed to José R. Dinneny
- 393 (dinneny@stanford.edu).

MATERIALS AND METHODS

Plant Material and growth conditions

Arabidopsis thaliana Col-0 ecotype was used in this study. Sisymbrium irio was obtained from Chris Pires, University of Missouri (KM 88-34-20-14). Eutrema salsugineum ecotype Shandong and Schrenkiella parvula ecotype Lake Tuz were from Arabidopsis Biological Resource Center (CS22504 and CS22663, respectively).

Seeds were surface sterilized by washing in a 95% ethanol solution for 5-min in 1.5 mL Eppendorf tubes followed by a 5-min wash in a 20% bleach/ 0.1% Tween-20 solution with gentle rocking at each step. Seeds were then rinsed with sterile deionized water four times and stored in water for 7 days at 4°C in the dark.

After stratification, sterilized seeds were grown on 10 x 10 cm petri dish plates containing sterile 0.7% Gelzan media containing $\frac{1}{4}$ x MS nutrients (MSP01-50LT; Caisson), 1% sucrose, and 0.05% MES was adjusted to pH 5.7 with 1M KOH (this will be termed "standard media"). The media was then sterilized using a liquid cycle for 30 min. 60 mL of media was used per plate.

Seedlings were grown for 6 days before transfer to standard media supplemented with NaCl (Sigma-Aldrich) or ABA (Sigma- Aldrich). Methanol was used to dissolve and dilute ABA to a stock solution of 100 mM and added to standard media before pouring into plates. Growth of seedlings was performed in a Percival CU41L4 incubator at constant temperature 24'C with light conditions 14 h light and 10 h dark at 130 µmol m⁻² s⁻¹ light intensity. Plates were partially sealed with parafilm (Alcan Packaging) on three sides, while the top of the plate was sealed with micropore tape (3M) to allow for gas exchange. Plates were placed vertically in the chamber, so roots grow vertically along the surface of the media.

For root growth assays, 20-25 seeds were placed in a row across the plate with a 1000 mL pipette tip. After 6 days of growth under standard media conditions, the seedlings were transferred either to standard media plates again or to plates with supplements. The position of the root tip was marked at the time of transfer of the root to distinguish the development of the root before transfer and after transfer.

For tissues collected for NGS, sterilized mesh (about $10 \times 10 \text{ cm}$ squares) were first laid on the media plates. 3 rows of seeds (~100 seeds) were then plated using a 1000 mL pipette tip. The entire mesh would then be transferred with forceps to the plate after 6 days and the tissues were then separated at the root/shoot junction by a razor blade.

Phenotypic analysis of primary root growth

After seedlings are transferred to media containing various supplements, images of seedlings were captured using a CanonScan 9000F flatbed scanner (Canon). Images

were quantified using Fiji ⁴⁶. Scale was set as 237 pixels/cm and the image was measured using the segmented line tool. Two-way ANOVA and data visualization were done using R.

RNA-Seq library preparation and high-throughput sequencing

Total RNA was extracted from the root and shoot tissue using RNeasy plant mini kit (Qiagen 74904) according to the manufacturer's instructions for three biological replicates sampled from experiments performed on a separate day. RNA quantity was checked by Qubit (Q32852 Qubit® RNA Assay Kit). RNA quality of each sample was assessed with a 2100 Bioanalyzer (Agilent) and fragment analyzer. RNA-Seq libraries were made using NuGen Universal Plus mRNASeq according to the manufacturer's instructions. Lo Bind plastic was used at every step. AMPure XP Beads (Beckman Coulter, Cat A63987 or A63881) were used for the final purification steps. NuGen barcodes (Barcode Version: L2V22DR) were used for multiplexing. Samples were sequenced on Illumina NextSeq (single-read 75-bp run) with the multiplexed samples described above on 3 lanes.

DAP-Seq library preparation and high-throughput sequencing

The coding sequence of the ABF orthologs were identified using reciprocal blast and defined regions of synteny across species. Gateway cloning compatible primers will be designed to amplify each coding sequence from cDNA and clone the coding sequence into TOPO entry vectors ⁴⁷. Four nucleotides were added to the forward strand of the primer to facilitate directional cloning. After the reaction, the plasmids were transformed into chemically competent cells then grown overnight at 37°C. Colony PCR and sequencing were done to validate the cloned sequence. The confirmed entry clones were then recombined into a destination vector with LR clonase to generate a vector with an N-terminal HaloTag that is translationally fused to ABF. The HaloTag is a mutated hydrolase that covalently binds to Halolink resin which allows for stringent washing and the generation of an affinity matrix with the transcription factor 48. We found that using rabbit reticulocyte (TnT® T7 Coupled Reticulocyte Lysate System, Recombinant RNasin® Ribonuclease Inhibitor- Promega) instead of wheat germ extract for in vitro transcription and translation of the ABFs significantly reduces the background noise and increased the quality of peaks that are able to be pulled down from DAP-Seq. To confirm the successful expression and synthesis of each ABF, an immunoblot with anti-halo antibody (Anti-HaloTag® Monoclonal Antibody-Promega) was performed to confirm protein expression and binding efficiency for each TF. This ensures at least 50 ng of protein was used for each DAP-Seg pull down.

The quality of the TF- affinity matrix was assayed by using western blots to quantify the abundance of the TF before and after binding to the affinity matrix. GST-Halo was used

as a protein standard (Promega). Incubate 1 µL of reticulocyte extract before binding with beads and 2 µL of extract after the binding was used for each western on a precast gel (4–20% Criterion™ TGX™ Precast Midi Protein Gel, 12+2 well, 45 µl, BioRad). Before loading, Samples were mixed with Lamneii buffer and heated for 5 min at 95'C. Samples were run at 20 mA for 30 min then at 100 V until the bottom was reached. 5x Running buffer is made using Tris 15.1 g, Glycine 94 g, 50 mL 10% SDS. After running, proteins were transferred onto the nitrocellulose membrane using a midrange, semi-dry system (invitrogen). 10X TBS- 1L (80 g NaCl, 2 g KCL, 30 g Tris base, pH 8 with HCL autoclave for 30 min was diluted to 1X TBST with 0.05% Tween-20 and sodium azide. This was mixed with milk powder to make a 5% blocking buffer. The membrane was blocked for at least 1 hour at room temperature or overnight at 4°C. After 152 blocking. 10 µL of anti-halo was added to 15mL blocking buffer (10 µg) for primary antibody incubation. After incubation, the membrane was washed 5x for 5 min each in 1x TBST. The membrane was then incubated for 1 hour with secondary anti-mouse- HRP 1:10,000 in 5% milk-TBST (2 µL in 20 mL blocking buffer). The membrane was washed again 5x for 5 min each in 1x TBST. Chemiluminescent reagent in 1:1 ratio was added to the membrane afterward and Chemi (ECL) signal was detected using Sapphire biomolecular imager. Image processing and labeling was done in Fiji.

Shoot tissues from 6-day old seedlings were used to generate the genomic DNA library. gDNA was extracted from root and shoot tissue by grinding tissues with cold mortar and pestle then using DNeasy Plant Maxi Kit (Qiagen). gDNA was then concentrated using ethanol precipitation. gDNA was incubated for 10-15 min with 10% NaOAC, 200% cold 100% ethanol. After precipitation, the sample was washed with 80% ethanol then dried into a pellet then redissolved. gDNA was fractionated using the COVARIS system under the settings (mode: Frequency sweeping, Duty cycle: 10%, intensity: 5, Cycles burst: 200, Time: 60 seconds, and number of cycles: 3). Another round of ethanol precipitation is done in the same manner as above. End repair (End-it kit; epicentre cat # ER0720 or ER81050- we used this one) and A-tailing (100mM dATP; bioPioneer inc, Klenow; (3'- 5' exo- NEB) # M0212L (1,000 units) (5,000 U/mL) was done prior to ligating fractionated gDNA with partial next-generation sequencing adaptors using Y adaptors. Y adaptors were made by combining Adapter A with Adapter B then incubating the oligo mixture to 86'C for 2 minutes before allowing the reaction to return to room temperature.

Quality of DAP library was assayed using qPCR. 2 μ L of (5 ng/ μ L) DNA template was added to 18 μ L master mix made with 4 μ L Phusion high Fidelity DNA polymerase (M0530S, ThermoFisher), 1 μ L of 10 mM dNTP, 0.4 μ L of 10mM Illumina TruSeq Universal primer and TruSeq Index primer, Phusion enzyme, 10x SYBR Green I (diluted in DMSO), and H2O. DNA without adaptor ligation and water is used as a negative control. Each sample was repeated 3x and on 384 qPCR plates. Thermocycling settings

- were 2 min at 95'C, 30s at 98'C, 30 cycles of (15s at 98'C, 30 s at 60'C, 1 min at 72'C), followed by hold at 4'C. Quality of the library was assessed by looking at the amplification curve by plotting the curves in excel as CT vs relative fluorescence unit (RFU). If the curve plateaus within 10 cycles, then the library is good. However, if the curve plateaus after 20 cycles, then the library will not work in the final sequencing.
 - Final DNA is quantified using Qubit (broad range) and incubated with the ABF affinity matrix (Magne HaloTag beads, 20% slurry, promega, G7281 Lot 000243828, PBS, Ph 7.4 (homemade): Dissolve 8 g NaCl, 0.2 g KCL, 1.44g Na2HPO4 and 0.24 g KH2PO4 in 800 mL sterile water. Adjust pH to 7.4 with HCL. Add water to 1 liter and sterilize by autoclaving. Add 200 μ L of 25 % NP40 and mix well., Magnetic rack, DYNAL magnetic bead separations, Invitrogen) to pull down genomic DNA that bind to each ABF.
 - Full adaptors containing unique 6 bp barcodes was ligated to each eluted fraction of gDNA and multiplexed for high-throughput Next-generation sequencing. These were originally designed by Muching Yee. Samples were sequenced on Illumina Hi-Seq (paired-read 150-bp run) with the multiplexed samples.

Genomes and the use of genomes for bioinformatic analysis

The genomes and gene models for *A. thaliana* was obtained from TAIR (Araport11), while genomes and gene models for *S. parvula* (version 2.2) and *E. salsugineum* (version 1.0) were from Phytozome (Phytozome ID 574 and 173, respectively). For *S. irio*, we updated the previously published gene models ¹⁰ with an updated version using evidence-assisted *ab initio* gene model prediction by the MAKER v. 2.31.10 (https://www.yandell-lab.org/software/maker.html) based on *S. irio* BUSCO-trained parameters ⁴⁹ and RNA-seq data from the current study.

RNA-Seq data analysis

Raw reads were filtered and trimmed using TRIMGALORE which also generated FASTQ files for each of the libraries. Filtered reads were aligned to the reference genome using HISAT2 v. 2.2 and the expression of each primary gene model was estimated with StringTie v. 2.0.1 with default parameters⁵⁰. Differentially expressed genes were estimated using DESeq2⁵¹. For comparative analyses, primary protein-coding gene models from the four species were compared using CLfinder pipeline⁵² with MMSeqs2⁵³ as the aligner, to identify ortholog pairs and groups between pairs of species as well as for all four species. Gene Ontology (GO) annotation for *A. thaliana* was obtained on July 1st, 2020, from the GO consortium (http://geneontology.org/). For non-*Arabidopsis* species, protein-coding gene models that cover more than 70% of an *Arabidopsis* protein with alignment identified by MMSeqs2 with maximum sensitivity ('mmseqs -S 7.5' and e-value <0.001) were considered sharing the GO annotation with

the *Arabidopsis* protein. We used BiNGO⁵⁴ to identify GO terms enriched in up- and down-regulated DEGs. Redundant GO terms sharing more than 80% of their members were further consolidated using the GOMCL pipeline⁵⁵.

For Phylogenetically informed Profiling, we calculated Spearman's rank correlation of the fold-change of ABA responses for all ortholog pairs annotated with a GO term, between a pair of species. The significance of positive correlation was estimated for all pairs of species, using scipy.stats.spearmanr ⁵⁶ and subsequently corrected for multiple testing (Bejamini-Hochberg) for all GO terms and all RNA-seq samples. Genes without a DEG among their ortholog pair partners in all species, genes failed to pass the Cook's distance test by DESeq2 ⁵¹, and genes showing larger than 2-fold changes with adjusted *P*-value>0.05 (DESeq2), were excluded from the analysis. The matrix of presence or absence of positive correlation between orthologs were superimposed to the species tree, generated using the Agalma pipeline ⁵⁷, to identify function- and lineage(s)-specific modifications in gene regulations.

DAP-Seq data analysis

At least 5 million reads per each sample were filtered to remove adaptors, low-quality reads, and reads mapping to multiple locations and aligned to respective genomes using Bowtie (version 2.3). GEM version 3.4 was used for peak calling after normalizing libraries to both input and empty vector controls. Only peaks with q-value <0.01 was used for peak annotation.

For each ABF in each species, DAP-seq peaks from different biological replicates whose center positions were within three nucleotides from each other were merged with 'bedtools merge' (https://bedtools.readthedocs.io/). We considered merged DAP-seq peaks supported by minimum two biological replicates as high-confident ABF-binding sites, and counted their occurrences, as well as co-occurrence of their center positions with an ACGT-core or ABRE motif, within the 1~1kb (proximal) or 1001~2Kb (distal) regions of the 5' and 3' side of each primary protein-coding gene models, using a custom script (https://github.com/dinnenylab/BrassicaceaeGRN). The coordinates of all high-confident ABF-binding sites are available as Supplementary Dataset 6. For determining co-occupancy of DAP-seq peak positions by different ABFs (e.g. in swap DAP-seq experiment), we selected two to three replicates with comparable library sizes and ranked all peaks based on the sum of -log₁₀ (q-values) and normalized peak heights estimated by GEM across all selected replicates.

Designing primers

Primers were designed to amplify the CDS from different species. TM calculator was used to check that the TM is under 72'C and within 1-2'C apart from each other. CACC

was added to the 5' end of the forward primer to make the PCR product compatible with gateway cloning. The reverse complement of the reverse primer was checked to make sure it is not complementing with overhanging sequence GTGG at the 5'end. To make sure that the fused product is going to be in-frame, plasmid maps were 160 generated and the sequence from the ATG of the protein to VP16 was translated using Expasy protein translation. Primers were ordered from IDT and diluted to 100µM with sterile water prior to use.

Gene regulatory network

595596

597

598 599

600

601

602 603

604

605

606

607

608

609

610

611

612

613

614

615

616

617

618

619

620

621

622 623

624

To construct the gene regulatory network (GRN), we first manually curated a list of genes that were involved in the perception, biosynthesis and signaling of the different hormones (ABA, ethylene and auxin) as well as genes that were involved in the control of cell elongation and root growth by auxin and ethylene. Among these genes, only those with orthologs in the four species were considered for further analysis. The GRN was constructed using BioTapestry with genes that showed a significant fold change in response to ABA in at least one of the four species according to Supplementary Dataset S1. To construct the GRN regulatory network for S. parvula, we first identified genes that showed high-confidence ABF-binding, as defined in Supplementary Dataset S1, in either A. thaliana or S. parvula or in both. The changes in ABF binding are represented based on comparison to A. thaliana. For example, if a locus exhibited the presence of an ABF DAP-seg peak in A. thaliana but lacked an ABF DAP-seg peak in S. parvula, this was considered to be a loss of ABF binding (dotted lines). On the other hand, the absence of a peak in A. thaliana but presence in S. parvula at an orthologous locus was considered to be a gain in ABF binding (thick lines). The changes in position or number of DAP-seg peaks were not considered for this analysis. Based on these criteria, we identified changes in ABF binding that were specific to S. parvula and those that were present in other species of lineage II. The GRNs were constructed using Biotapestry.

References:

- Macneil, L. T. & Walhout, A. J. M. Gene regulatory networks and the role of robustness and stochasticity in the control of gene expression. *Genome Res.* 21, 645–657 (2011).
- Kazachkova, Y. *et al.* Halophytism: What Have We Learnt From *Arabidopsis thaliana* Relative Model Systems? *Plant Physiol.* 178, 972–988 (2018).
- 3. Raza, A. *et al.* Impact of Climate Change on Crops Adaptation and Strategies to Tackle Its Outcome: A Review. *Plants* **8**, (2019).
- 632 4. Shamustakimova, A. O., Leonova, T. G., Taranov, V. V., de Boer, A. H. & Babakov,

- A. V. Cold stress increases salt tolerance of the extremophytes *Eutrema*
- salsugineum (Thellungiella salsuginea) and Eutrema (Thellungiella) botschantzevii.
- 635 *J. Plant Physiol.* **208**, 128–138 (2017).
- 5. Mishra, A. & Tanna, B. Halophytes: Potential Resources for Salt Stress Tolerance Genes and Promoters. *Front. Plant Sci.* **8**, 829 (2017).
- 638 6. Yang, R. *et al.* The Reference Genome of the Halophytic Plant *Eutrema* salsugineum. Front. Plant Sci. **4**, 46 (2013).
- 7. Dassanayake, M. *et al.* The genome of the extremophile crucifer *Thellungiella parvula. Nat. Genet.* **43**, 913–918 (2011).
- 642 8. Oh, D.-H. *et al.* Genome Structures and Transcriptomes Signify Niche Adaptation 643 for the Multiple-Ion-Tolerant Extremophyte *Schrenkiella parvula*. *Plant Physiology* 644 vol. 164 2123–2138 (2014).
- 9. MacLeod, M. J. R. *et al.* Exposure of two *Eutrema salsugineum* (*Thellungiella salsuginea*) accessions to water deficits reveals different coping strategies in response to drought. *Physiol. Plant.* **155**, 267–280 (2015).
- 10. Haudry, A. *et al.* An atlas of over 90,000 conserved noncoding sequences provides insight into crucifer regulatory regions. *Nat. Genet.* **45**, 891–898 (2013).
- 11. Wang, J. *et al.* Genome-Wide Analysis of Gene Expression Provides New Insights into Cold Responses in Thellungiella salsuginea. *Front. Plant Sci.* **8**, 713 (2017).
- 12. Orsini, F. *et al.* A comparative study of salt tolerance parameters in 11 wild relatives of *Arabidopsis thaliana*. *J. Exp. Bot.* **61**, 3787–3798 (2010).
- 13. Xuejie, W. X. Z. P. Z. & Shoujin, Z. L. F. COMPARATIVE STUDIES ON GROWTH
 AND PHYSIOLOGICAL REACTION OF THELLUNGIELLA SALSUGINEA UNDER
 NaCI AND Na_2SO_4 STRESSES [J]. Journal of Shandong Normal University
 (Natural Science) 1, (2007).
- 14. Lee, Y. P. *et al.* Salt stress responses in a geographically diverse collection of Eutrema/Thellungiella spp. accessions. *Funct. Plant Biol.* **43**, 590–606 (2016).
- 15. Cutler, S. R., Rodriguez, P. L., Finkelstein, R. R. & Abrams, S. R. Abscisic acid: emergence of a core signaling network. *Annu. Rev. Plant Biol.* **61**, 651–679 (2010).
- 16. Sah, S. K., Reddy, K. R. & Li, J. Abscisic Acid and Abiotic Stress Tolerance in Crop Plants. *Front. Plant Sci.* **7**, 571 (2016).
- 17. Vishwakarma, K. et al. Abscisic Acid Signaling and Abiotic Stress Tolerance in
 Plants: A Review on Current Knowledge and Future Prospects. Front. Plant Sci. 8,
 161 (2017).
- 18. Yoshida, T. *et al.* Fou*rArabidopsis* AREB/ABF transcription factors function predominantly in gene expression downstream of SnRK2 kinases in abscisic acid

- signalling in response to osmotic stress. *Plant, Cell & Environment* vol. 38 35–49 (2015).
- 19. Yamaguchi-Shinozaki, K. & Shinozaki, K. A novel cis-acting element in an Arabidopsis gene is involved in responsiveness to drought, low-temperature, or high-salt stress. *Plant Cell* **6**, 251–264 (1994).
- 20. Sun, Y. & Dinneny, J. R. Q&A: How do gene regulatory networks control environmental responses in plants? *BMC Biol.* **16**, 38 (2018).
- 21. Deprost, D. *et al.* The *Arabidopsis* TOR kinase links plant growth, yield, stress resistance and mRNA translation. *EMBO Rep.* **8**, 864–870 (2007).
- 678 22. Fornes, O. *et al.* JASPAR 2020: update of the open-access database of transcription factor binding profiles. *Nucleic Acids Research* (2019) doi:10.1093/nar/gkz1001.
- 681 23. O'Malley, R. C. *et al.* Cistrome and Epicistrome Features Shape the Regulatory DNA Landscape. *Cell* **165**, 1280–1292 (2016).
- 683 24. Guo, Y., Mahony, S. & Gifford, D. K. High resolution genome wide binding event finding and motif discovery reveals transcription factor spatial binding constraints.

 685 *PLoS Comput. Biol.* **8**, e1002638 (2012).
- Vyse, K., Pagter, M., Zuther, E. & Hincha, D. K. Deacclimation after cold
 acclimation-a crucial, but widely neglected part of plant winter survival. *J. Exp. Bot.*70, 4595–4604 (2019).
- 26. Song, L. *et al.* A transcription factor hierarchy defines an environmental stress response network. *Science* **354**, (2016).
- 691 27. Thole, J. M., Beisner, E. R., Liu, J., Venkova, S. V. & Strader, L. C. Abscisic acid 692 regulates root elongation through the activities of auxin and ethylene in *Arabidopsis* 693 *thaliana*. *G* **3 4**, 1259–1274 (2014).
- Rowe, J. H., Topping, J. F., Liu, J. & Lindsey, K. Abscisic acid regulates root growth under osmotic stress conditions via an interacting hormonal network with cytokinin, ethylene and auxin. *New Phytol.* **211**, 225–239 (2016).
- 29. Qin, H., He, L. & Huang, R. The Coordination of Ethylene and Other Hormones in Primary Root Development. *Front. Plant Sci.* **10**, 874 (2019).
- 30. Majda, M. & Robert, S. The Role of Auxin in Cell Wall Expansion. *Int. J. Mol. Sci.* 19, (2018).
- 31. Strader, L. C., Chen, G. L. & Bartel, B. Ethylene directs auxin to control root cell expansion. *Plant J.* **64**, 874–884 (2010).
- 32. Li, J., Xu, H.-H., Liu, W.-C., Zhang, X.-W. & Lu, Y.-T. Ethylene Inhibits Root
 Elongation during Alkaline Stress through AUXIN1 and Associated Changes in

- 705 Auxin Accumulation. *Plant Physiol.* **168**, 1777–1791 (2015).
- 706 33. Takatsuka, H. & Umeda, M. Hormonal control of cell division and elongation along differentiation trajectories in roots. *J. Exp. Bot.* **65**, 2633–2643 (2014).
- 708 34. Mao, J.-L. *et al. Arabidopsis* ERF1 Mediates Cross-Talk between Ethylene and
 709 Auxin Biosynthesis during Primary Root Elongation by Regulating ASA1
 710 Expression. *PLoS Genet.* 12, e1005760 (2016).
- 711 35. Van den Broeck, L. *et al.* From network to phenotype: the dynamic wiring of an *Arabidopsis* transcriptional network induced by osmotic stress. *Mol. Syst. Biol.* **13**, 961 (2017).
- 714 36. Yang, Z., Tian, L., Latoszek-Green, M., Brown, D. & Wu, K. *Arabidopsis* ERF4 is a transcriptional repressor capable of modulating ethylene and abscisic acid responses. *Plant Mol. Biol.* **58**, 585–596 (2005).
- 717 37. Dubois, M. *et al.* Ethylene Response Factor6 acts as a central regulator of leaf 718 growth under water-limiting conditions in *Arabidopsis*. *Plant Physiol*. **162**, 319–332 719 (2013).
- 38. Müller, M. & Munné-Bosch, S. Ethylene Response Factors: A Key Regulatory Hub in Hormone and Stress Signaling. *Plant Physiol.* **169**, 32–41 (2015).
- 39. Markakis, M. N. *et al.* Identification of genes involved in the ACC-mediated control of root cell elongation in *Arabidopsis thaliana*. *BMC Plant Biol.* **12**, 208 (2012).
- 40. Miao, Z.-Q. *et al.* HOMEOBOX PROTEIN52 Mediates the Crosstalk between
 Ethylene and Auxin Signaling during Primary Root Elongation by Modulating Auxin
 Transport-Related Gene Expression. *Plant Cell* 30, 2761–2778 (2018).
- 41. Velasquez, S. M., Barbez, E., Kleine-Vehn, J. & Estevez, J. M. Auxin and Cellular Elongation. *Plant Physiol.* **170**, 1206–1215 (2016).
- 729 42. Pacheco-Villalobos, D., Sankar, M., Ljung, K. & Hardtke, C. S. Disturbed local auxin homeostasis enhances cellular anisotropy and reveals alternative wiring of auxin-ethylene crosstalk in Brachypodium distachyon seminal roots. *PLoS Genet.* 732 **9**, e1003564 (2013).
- 733 43. Thole, J. M., Beisner, E. R., Liu, J., Venkova, S. V. & Strader, L. C. Abscisic acid 734 regulates root elongation through the activities of auxin and ethylene in *Arabidopsis* 735 *thaliana*. *G3: Genes, Genomes, Genetics* **4**, 1259–1274 (2014).
- 44. Stepanova, A. N. *et al.* TAA1-mediated auxin biosynthesis is essential for hormone crosstalk and plant development. *Cell* **133**, 177–191 (2008).
- 738 45. Rodríguez-Leal, D., Lemmon, Z. H., Man, J., Bartlett, M. E. & Lippman, Z. B.
 739 Engineering Quantitative Trait Variation for Crop Improvement by Genome Editing.
 740 Cell 171, 470–480.e8 (2017).

- 741 46. Schindelin, J. *et al.* Fiji: an open-source platform for biological-image analysis. *Nat. Methods* 9, 676–682 (2012).
- 743 47. Patel, B. Simple, Fast, and Efficient Cloning of PCR Products with TOPO® Cloning Vectors. *BioTechniques* vol. 46 559 (2009).
- 48. England, C. G., Luo, H. & Cai, W. HaloTag technology: a versatile platform for biomedical applications. *Bioconjug. Chem.* **26**, 975–986 (2015).
- 747 49. Waterhouse, R. M. *et al.* BUSCO Applications from Quality Assessments to Gene Prediction and Phylogenomics. *Mol. Biol. Evol.* **35**, 543–548 (2018).
- 749 50. Pertea, M., Kim, D., Pertea, G. M., Leek, J. T. & Salzberg, S. L. Transcript-level 750 expression analysis of RNA-seq experiments with HISAT, StringTie and Ballgown. 751 *Nat. Protoc.* **11**, 1650–1667 (2016).
- 51. Love, M. I., Huber, W. & Anders, S. Moderated estimation of fold change and dispersion for RNA-seq data with DESeq2. *Genome Biol.* **15**, 550 (2014).
- 52. Oh, D.-H. & Dassanayake, M. Landscape of gene transposition-duplication within the Brassicaceae family. *DNA Res.* **26**, 21–36 (2019).
- 53. Steinegger, M. & Söding, J. MMseqs2 enables sensitive protein sequence searching for the analysis of massive data sets. *Nat. Biotechnol.* **35**, 1026–1028 (2017).
- Maere, S., Heymans, K. & Kuiper, M. BiNGO: a Cytoscape plugin to assess
 overrepresentation of gene ontology categories in biological networks.
 Bioinformatics 21, 3448–3449 (2005).
- 762 55. Wang, G., Oh, D.-H. & Dassanayake, M. GOMCL: a toolkit to cluster, evaluate, and
 763 extract non-redundant associations of Gene Ontology-based functions. *BMC* 764 *Bioinformatics* 21, 139 (2020).
- 56. Virtanen, P. *et al.* SciPy 1.0: fundamental algorithms for scientific computing in Python. *Nat. Methods* **17**, 261–272 (2020).
- 57. Dunn, C. W., Howison, M. & Zapata, F. Agalma: an automated phylogenomics workflow. *BMC Bioinformatics* **14**, 330 (2013).

Figure Legends

769 770

- 772 Fig.1: S. parvula responds differently to ABA. a, ABA signaling pathway in
- 773 Arabidopsis. ABA functions to regulate cellular and tissue level responses to
- environmental stress such as cold, salt, and drought. ABA signaling alters cellular
- responses by activating the transcription of many genes. **b**, A simplified phylogenetic
- tree representing an overview of how the diploid species from Brassicaceae relate to
- one another and a summary of their comparative genome size, number of

778

779

780

781 782

783

784

785

786

787

788

789

790 791

792

793

794

795

796

797

798

799

800

801

802

803

804

805

806

807

808

809

810

811

812

813

814

815

816

817

chromosomes, and number of coding sequences. **c,d,** Quantification of primary root growth of At, Si, Sp, and Es seedlings after transfer to media containing control, 100, 150, 200 mM NaCl (**c**), or 1, 5, 10 μ M ABA (**d**) for 2 days. Asterisks mark significant changes based on two-way ANOVA, *P < 0.05, **P < 0.01, ***P < 0.001, n>6. **e**, Confocal microscopy images of both At and Sp primary roots grown on standard media or media containing 10 μ M ABA. Blue bars label the stabilized cortex cell length. Red arrows point to the end of meristem. Scale bars = 100 μ m. **f**, Quantifications of root meristem size, by counting the total cortex cell number within the meristem, for both At and Sp under control and 1 or 10 μ M ABA treatment. Significance test is based on pairwise T-test, ***P < 0.001, n = 5. **g,h**, Quantification of cortex cell length for both At (**g**) and Sp (**h**) under control, 1 or 10 μ M ABA treatment (n = 5). The x-axis indicates cell number starting from the quiescent center (QC).

Fig.2: RNA-Seg identifies genes regulated by ABA across species. a, Bar chart summarizing the number of differentially expressed (DE) genes across species. Log₂ fold change was used to quantify the total number of up and down- regulated genes for each species. Only genes with a p-value <0.05 are displayed. Red indicates upregulated genes, blue indicates down-regulated genes. b, Heatmap of log₂ fold change of differentially expressed genes. Each species was clustered separately using Ward's hierarchical clustering method. Clusters are then arranged in descending order. c, Lists of DE genes from each species are compared with DE genes from Arabidopsis and categorized into 4 separate categories (1) Genes with ortholog in At. (2) Genes specific to species, (3) Genes specific to species with phenotypes in At, (4) Genes specific to species with unknown function. d, Cluster analysis of 1:1 Ortholog Groups (OGs) and number of genes associated with each pattern. Total 15,198 1:1 OGs were defined where all ortholog pairs were reciprocally best homologs among themselves (Supplementary Fig. 1) and used to associate differential gene expression. The top 9 categories of gene expression are shown in descending order. Pink indicates orthologous genes across species. e.f. Phylogenetically-informed profiling (Pip) highlights the regulatory traits that show the most significant lineage(s)-specific modifications. While ortholog pairs annotated with GO-term "response to abscisic acid" showed significant positive Spearman correlation (p) of ABA-responsive expression fold-changes (* adjusted p<10⁻⁷) in all species pairs (**e**), the correlation disappeared in GO term "peptide biosynthetic process" in species pairs including S. parvula (Sp), due to a subset of Sp genes regulated in the opposite direction (yellow arrows), signifying a lineage-specific modification (red arrow in the species tree) (f). Among all tested, conserved ABA-response (e) was the most frequent profile (3,424 GO-sample), while unique modification in Sp (f) was among the next most frequent (123 GO-sample) (Supplementary Fig. 3a). The GO term "peptide biosynthetic process" in root 3hr ABA treatment sample represents one of the biggest variance in p among larger GO terms

(Supplementary Fig. 3b) See Supplementary Dataset 4 for Pip results for all GO terms and samples.

818 819

820 821

822

823

824

825

826

827

828

829

830

831

832

833 834

835

836

837

838 839

840

841

842

843

844

845

846

847

848

849

850

851

852

853

854

855

856

857

Fig.3: Differences in the transcriptional response are partially due to differences in the ABF binding landscape across species. a, Experimental set up to profile differences in AREB/ABF function and target genes across species for DAP-Seq and Swap-Dap. The ABRE is the enriched motif under the peaks associated with ABF binding. 16 ABF orthologs are displayed based on the phylogenetic association of their amino acid sequence. For each ABF, the enriched motif is represented as a position weight matrix (PWM). b, Overlap of DAP-seg peak positions bound by ABFs. Upper panel shows overlaps among top 3000 DAP-seg peak positions in each Brassicaceae genome bound by ABF1/2/3/4. In the lower panel, ABFs from four Brassicaceae species were applied to the Arabidopsis thaliana genome in swap-DAP-seg experiments. Cooccupancy by ABFs from different species for top 1000 peak positions was plotted for each ABF. Top DAP-seq peak positions were identified by ranking based on the significance and normalized peak heights, as detailed in methods. A summary of how peaks overlaps over different numbers of top peak positions is in Supplementary Fig. 6. c, A genome browser summary to highlight an example gene where ABF binding is lost in Sp but not in other species, which correlates with gene expression differences. The gene IDs associated for each species are (At) AT2G21510.2, (Si) Si s2286 00530.m. (Sp) Sp4q00670.a, and (Es) Thhalv10000223m.v1.0. Y-axis on IGV coverage track is adjusted for each track to show the maximum height for the depth of coverage while the gene model is proportional to what is observed in a 10,000 bp window. For Sp tracks, yaxis was adjusted to the lower range of 50 to confirm no peaks were present. Panels show peak signal vs. empty vector and input control, differences in ABF binding across species, similarities in binding sites in swap-dap data, and corresponding gene expression data for transcripts. At, Si, and Es show positive log₂ fold change while Sp shows negative fold change upon ABA treatment. d, A nucleotide alignment of sequences in the 5' promoter of At, Si, Sp, and Es. The reverse complement was used for the alignment since the gene is in the reverse strand. Alignment was performed in MUltiple Sequence Comparison by Log- Expectation (muscle). Blue boxes highlight the ABRE motif. Red letter nucleotide change that leads to the mutation and loss of the core ABRE motif. e, We tested whether genes including a DAP-seq peak in different genomic regions were enriched among ABA-induced DEGs compared to genes not regulated by ABA (background). Percent enrichment, compared to background, for genes significantly ABA-induced in any of the four samples (up-DEG in any sample, i.e. root or shoot tissues treated with ABA for 3hr or 24hr) and in all four samples (up-DEG in all samples) were plotted separately. Genomic regions are divided into 5' distal (5pD), 5' proximal (5pP), genomic coding sequences (qCDS), 3' proximal (3pP), and 3' distal (3pD), where proximal regions are within 1Kb of the coding sequence of a gene model

and distal regions the next 1Kb blocks beyond the proximal regions. Significance of enrichment (g-test with Benjamini-Hochberg correction) was marked for adjusted p-value < 10⁻⁵ (*), <10⁻²⁰ (**), and <10⁻⁵⁰ (***). Significant enrichment of genes containing a DAP-seq peak in most genomic regions was not observed among ABA-repressed DEGs (**Supplementary Table 1**).

Missing BUSCOs

Fig.4: Rewiring of ABF-Auxin biosynthesis regulatory network is responsible for altered growth response in S. parvula. a, Gene regulatory network for auxin biosynthesis, transport, signaling, and cell wall are composed based on data from previous published literature. A list of binding sites from ABF 1-4 were consolidated to draw the gene network in Arabidopsis. Sp data was overlaid onto the Arabidopsis network. Species-specific differences are highlighted as well as the presence or absence of a peak based on ABF binding. **b**, Heatmap summarizing the RNA-Seq data across At and Sp for species-specific and lineage-specific data highlighted in previous GRN. Genes are clustered based on differences observed between At and other species. **c**, Quantification of primary root growth for WT and wei8-1 mutants treated with control, 1 μM ABA, as well as WT with 1μM L-Kyn, and 1 μM L-Kyn + 1 μM ABA. Asterisk indicate significance by 2-way ANOVA. ***P < 0.001, n>30. **d**, A schematic mechanism we proposed for the differential regulation in primary root growth in Sp compared with At.

Supplementary Fig.1: Genome versions used in current study and detection of all 1-to-1 ortholog groups.

a, The genome versions used as well as gene loci, percent of loci in large scaffolds, and the Benchmarking Universal Single-Copy Orthologs (BUSCOs) analysis are shown along with an updated gene model annotation for *Sisymbrium irio*. b, A schematic example of OrthNet constructed for the four crucifer species. Protein-coding gene models from each species were paired with their best homologs in other species. Pairs of homologs were organized into OrthNet, each OrthNet representing orthologs likely derived from a single ancestral locus (Oh and Dassanayake, 2019). Within each OrthNet, a quartet of orthologs unambiguously find each other as reciprocal best homologs is defined as "all 1-to-1 ortholog group (OG)" (red dashed box). We identified 15,198 all 1-to-1 OGs among the four crucifers, and used them as the framework for cross-species comparisons. RNA-seq and DAP-seq results for all 1-to-1 OGs are in Supplementary Dataset 1, while the same data for all genes, organized as OrthNets including all duplicated paralogs, are in Supplementary Dataset 2.

^a Percentage of 1,375 BUSCOs (embryophyte ortholog database version 10) detected in each genome; C, Complete; S, Single-copy; D, Duplicated; F, Fragmented; M,

^b Using the updated *S. irio* gene models, the number of unambiguous all-1-to-1 ortholog groups in the four crucifer species increased to 15,198, compared to 14,526 when the original version of *S. irio* gene models by Haudry, et al. (2013) was used.

Supplementary Fig.2: Enrichment of Gene Ontology (GO) term "response to abiotic stimulus" and related GO terms among ABA-induced Differentially Expressed Genes (DEGs). a, The GO term "response to abiotic stimulus" and ten related non-redundant GO terms (presented in the heatmap in the bottom panel) were the only GO terms showed significant enrichment among ABA-induced DEGs (up-DEGs) in all samples, i.e. 3hr ABA treatment, root tissue (R3); 24hr, root tissue (R24); 3hr, shoot tissue (S3); and 24hr, shoot tissue (S24) for all species, i.e. *Arabidopsis thaliana* (At), *Sisymbrium irio* (Si), *Schrenkiella parvula* (Sp), and *Eutrema salsugineum* (Es). The top panel shows the proportion of up-DEGs that are annotated with any of the "response to abiotic stimulus" and the ten related GO terms, compared to the mean proportion in all genes of the four species, i.e. the background (dashed line). Bottom panel shows the significance of enrichment, estimated with a hypergeometric test with Benjamini-Hochberg correction as a heatmap. The entire GO terms showing enrichment of any of the ABA-induced or repressed DEGs are compiled in Supplementary Dataset 3.

Supplementary Fig. 3: Phylogenetically informed Profiling (PiP) analysis of ABA-responses

1.a, For all non-redundant GO terms, we determined if there is a significant positive Spearman correlation (+corr) of ABA responses among ortholog pairs for all six pairs of the four species, i.e. Arabidopsis thaliana (At), Sisymbrium irio (Si), Schrenkiella parvula (Sp), and Eutrema salsugineum (Es). The matrix of presence (1) and absence (0) of +corr was calculated for ABA-responsive fold change of gene expression in each of the four samples, i.e. root and shoot tissues with 3 and 24hr ABA treatment. In panel a, we show the number of GO-sample pairs with the indicated +corr patterns across all pairs of species. The most frequent +corr pattern (3,425 GO-sample pairs) represented GOsample pairs with no modification in any lineage ("Conserved in all"). The next dominant +corr pattern (123 GO-sample pairs) that matches a phylogenetic profile showed a modification of ABA responses uniquely in Sp ("Unique@Sp"). Phylogenetic profiles "AtEs-SiSp" mirrors the divergence of Si and Sp clades from the other two species. while "AtSi-vs-SpEs" indicates potential division between glycophytes (At and Si) and halophytes (Sp and Es). For all GO-sample pairs, we plotted the Variance of Spearman correlation coefficients among the six species pairs against the number of ortholog pairs used for PiP analyses. b. While in general the magnitude of variance was greater for smaller GO terms, "peptide biosynthetic process" and related GO terms at root 3hr ABA

treatment samples were outliers with greater variances among larger GO terms (marked red). Results of PiP analysis for all GO-sample pairs are in Supplementary Dataset 4.

Supplementary Fig. 4: Transcription factor (TF)-binding motifs enriched among ABA-induced DEGs. a, For the 1Kb upstream regions of all ABA-induced and repressed DEGs, we searched for enrichment of known TF-binding motifs (from JASPAR database). The four ABFs and other G-box-binding TFs (G-box TFs) were the only TFs whose known binding motifs showed significant enrichment (determined using AME) in promoters of ABA-induced DEG promoters in all samples. **b,** Proportion of promoters including an ABF or G-box TF-binding motif is shown in panel b, for both DEGs ABA-induced (Up-DEGs) and repressed (Down-DEGs), with the mean proportion among non-DEGS shown as dotted lines (G-Box TF) and dashed lines (ABFs). The enrichment profiles of all JASPAR TF-binding motifs are in Supplementary Dataset 5.

Supplementary Fig.5: AREB/ABFs of different species cluster together based on protein sequence and have conserved DNA-binding and protein-protein interaction domains. a, Alignment was generated using CLUSTALW with the amino acid sequences for each species. Black box highlights the conservation of the DNA binding domain and the protein-protein interaction domain for ABFs across species.

Supplementary Fig.6: Quality control checks to confirm the DAP-Seq assay works as expected. a, DAP-Seq peaks associated with ABI1 and RD29A, which are marker genes for ABA response, are found across all species. Genome browser view shows binding sites represented as "peaks". Dotted lines connect orthologous genes across species. ABREs are labeled in red and the data range for X axis was standardized to 10,000bp. Corresponding differential gene expression data (ABA treatment vs. control from RNA-Seq for each gene ortholog across species is shown as log₂ fold change. **b**, Proteins synthesized by in vitro transcription/ translation (IVT) runs to expected size within typical yields as described in O'Malley *et al.* anti-HALO monoclonal antisera was used for detection of HALOtag used to generate the affinity matrix. GST-HALOTag (Halo protein) was used as positive control.

Supplementary Fig.7: Distribution of ACGT and ABRE motifs and proportions occupied by a DAP-seq peak. a, On the left panels, occurrences per kilobase (Kb) of the ACGT, ACGT sequences that are not a part of an ABRE (ACGT – ABRE), and ABRE motif, are plotted for different genomic regions adjacent to protein-coding gene models. Genomic regions are divided into 5' distal (5pD), 5' proximal (5pP), genomic coding sequences (gCDS), 3' proximal (3pP), and 3' distal (3pD), where proximal regions are within 1Kb of the coding sequence of a gene model and distal regions the next 1Kb blocks beyond the 1Kb regions. Intergenic regions are those not within 2Kb of

any gene model. For each motif, percent proportions occupied by an ABF-binding DAP-seq peak are shown on the right panel. Motif logos indicate the definition of ACGT and ABRE motif. Genomic coordinates of all high-confidence DAP-seq peaks, together with their coincidence with ACGT or ABRE motifs and genomic regions adjacent to protein-coding gene models, are in Supplementary Dataset 6.

Supplementary Fig. 8: Ranks and overlap of DAP-seq peaks. a, DAP-seq peaks were ranked based on significance and peak heights as detailed in Methods. We selected the top N ranked DAP-seq peaks from each experiment and compared their overlaps among ABF1/2/3/4 within each species (A) or among ABF orthologs derived from At/Si/Sp/Es for each ABF in swap DAP-seq experiment. **b,** Percentages of DAP-seq peak positions shared by all four ABFs (intersection) among all peak positions (union) were plotted over different N values.

Supplementary Fig.9: ABF binding in AT5G42570 and orthologs across species is lost in *S. parvula*.

a, genome browser view showing binding sites represented as "peaks". Data shows loss of binding in Sp compared to binding in all other samples. The gene IDs associated for each species are (At) AT5G42570, (Si) Si_s118_00070.m, (Sp) SpUn0014_0110, and (Es) Thhalv10003268m.v1.0. Y-axis on IGV coverage track is adjusted for each track to show the maximum height for the depth of coverage while the gene model is proportional to what is observed in a 10,000 bp window. For Sp tracks, y-axis was adjusted to the lower range of 50 to confirm no peaks were present. Swap-DAP data indicates the peak loss is due to cis since SpABFs are able to bind to the 5' promoter region in the At genome. RNA-Seq data corresponds to peak patterns where the presence of a peak suggests transcriptional activation.

Supplementary Fig.10: Core ABRE is mutated in Sp ortholog of AT5G42570 a, An alignment of sequences in the promoters of AT5G42570 and corresponding orthologs. The reverse complement for each sequence was taken since genes are in the reverse strand then aligned with MUltiple Sequence Comparison by Log-Expectation (muscle). Blue boxes indicate the ABRE motif, the red letter indicate the nucleotide sequence change in Sp at the ABRE leading to the loss of the binding site for Sp.

Supplementary Fig.11: Integration of ABF transcription factors into hormone (ABA and Ethylene) gene regulatory networks in *S. parvu*la. Gene regulatory maps were drawn using BioTapestry, with a solid arrow line indicating correlation between ABF binding (DAP-Seq) and gene expression (RNA-Seq). a, A Map for *Arabidopsis* ABF-mediated gene regulatory network was drawn with overlapping transcription factors

and targets from ChIP-Seq (Song et al., 2016). DAP-Seq and RNA-Seq data from different species were overlaid and differences are highlighted: dotted arrow indicates loss of ABF binding, bold arrow indicates gain of ABF binding, and colors indicate differences that are lineage II specific, Sp-Si specific, Sp-Es specific, or Sp specific. Heatmap indicates differential gene expression patterns in all tissue types and time points for all nodes used to construct the GRN. **b**, An overlay of ABF-mediated GRN using ethylene regulatory network curated from previously published literature is shown. Of the 72 genes identified, 50 were responsive to ABA, and 33 had ABF DAP peaks in either At, Sp, or both which were used to construct the GRN. Among these however, only 2 were specific to Sp (ACS7 and ERF2) while the other 20 showed lineage II, Sp-Es, or Sp-Si specific differences. Heatmap indicates differential gene expression patterns in all tissue types and time points for all nodes used to construct the GRN. LFC2 indicates log2 fold change.

Supplementary Fig.12: Comparison between *A. thaliana* and *S. parvula* data sets reveal changes in ABF mediated auxin gene regulatory network. a, A total of 199 genes were curated for the analysis. 117 of the 199 genes related to primary auxin signaling in roots were present in our RNA-Seq data. 81 of these genes had ABF DAP peaks in either At or Sp or in both suggesting ABF mediate gene regulation and shown in this GRN as nodes. The same parameters were used as in Supplementary Fig.8 to highlight lineage, Sp-Si, Sp-Es, or Sp specific differences compared to At.

Figure 1: S. parvula responds differently to ABA.

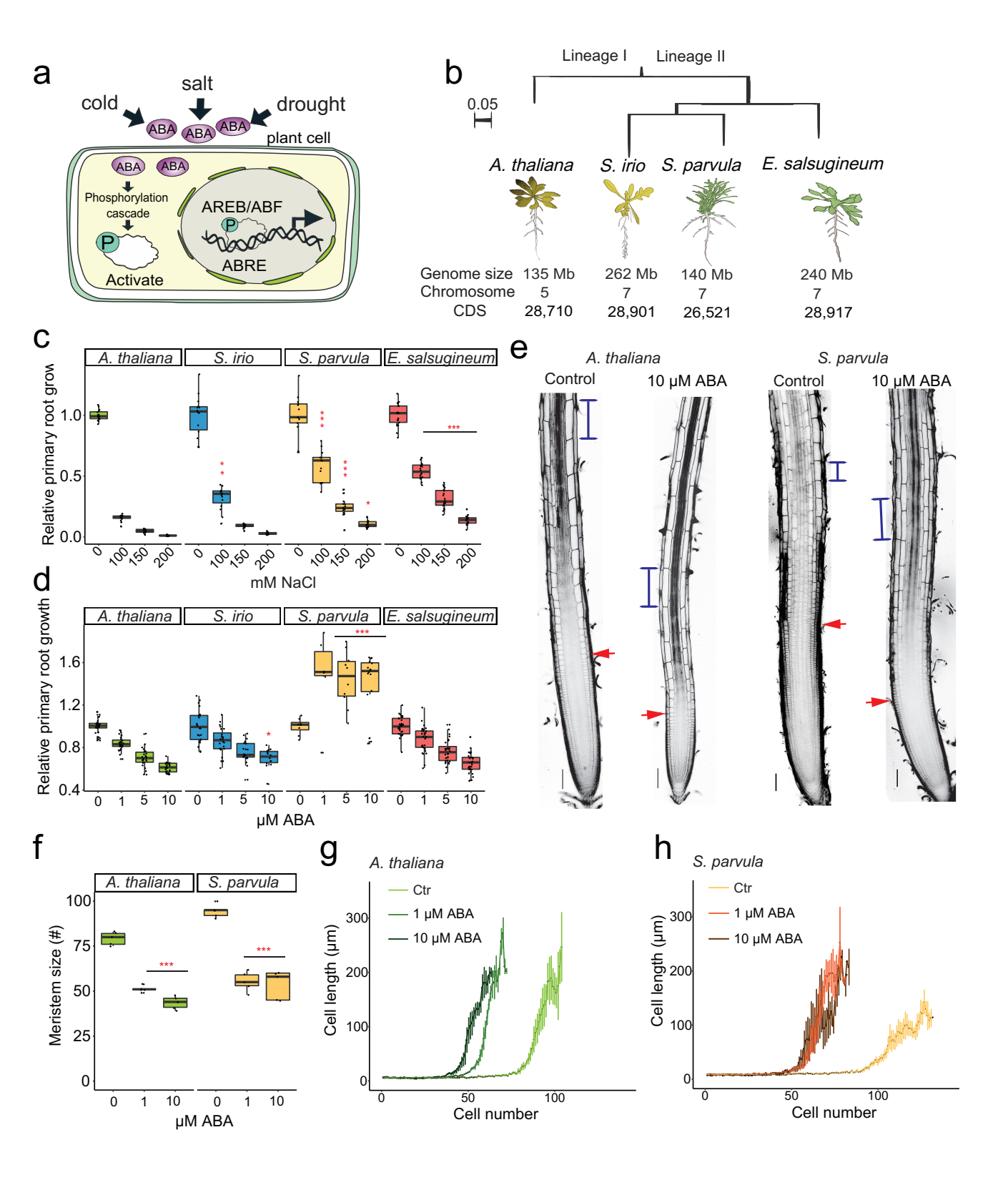


Figure 2: RNA-Seq identifies genes regulated by ABA across species.

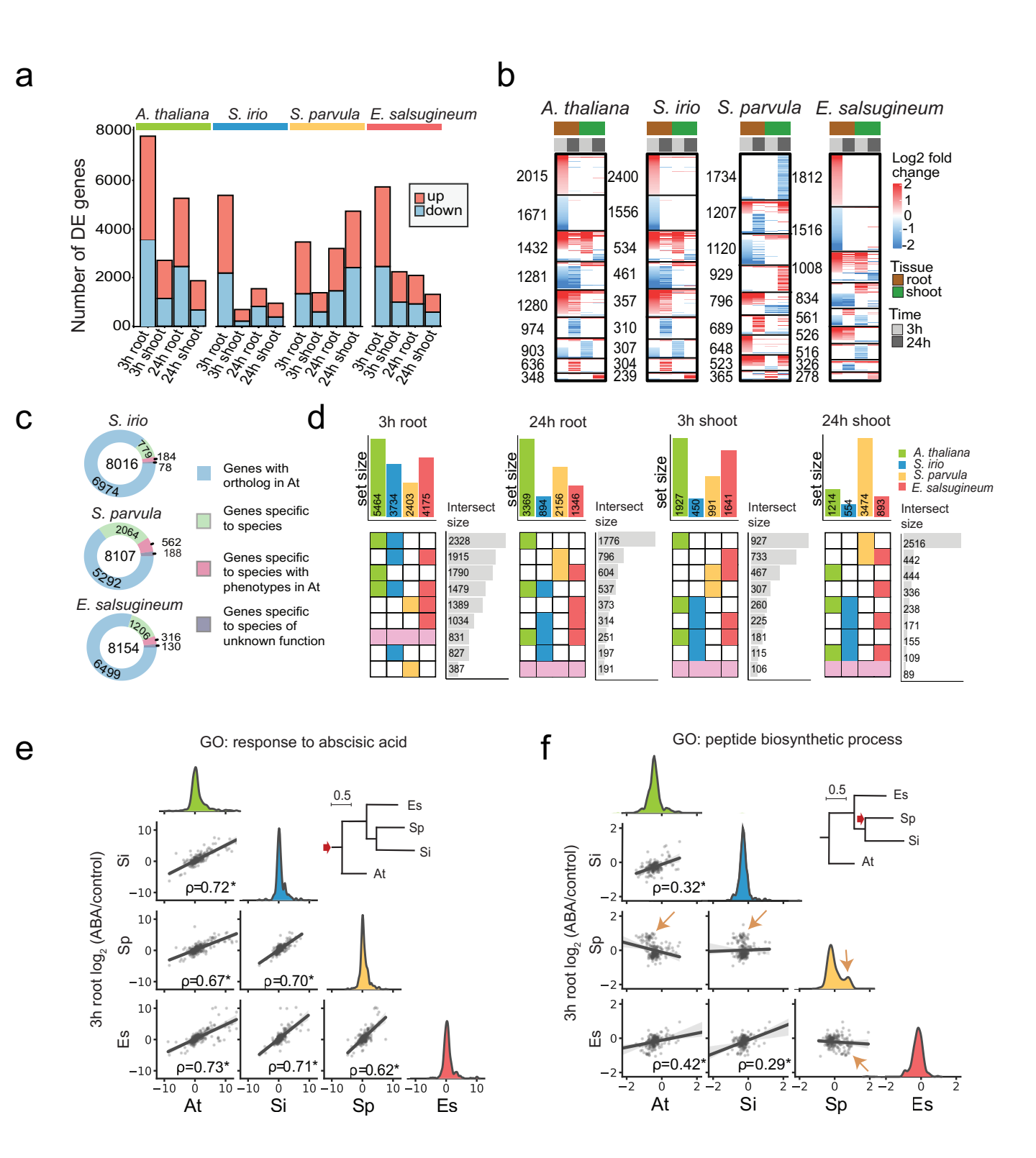


Figure 3: Differences in the transcriptional response are partially due to differences in the AREB/ABF binding landscape across species.

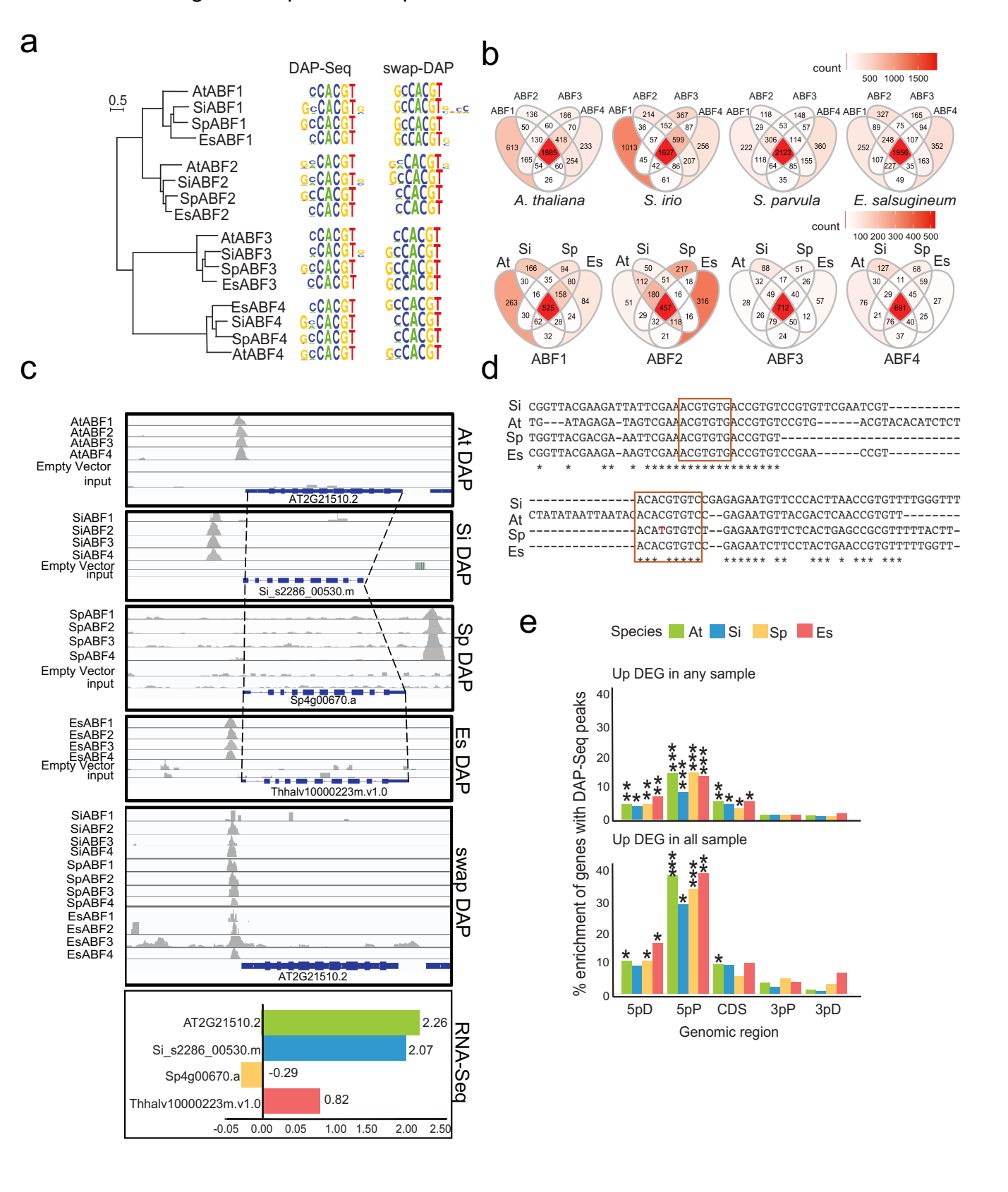
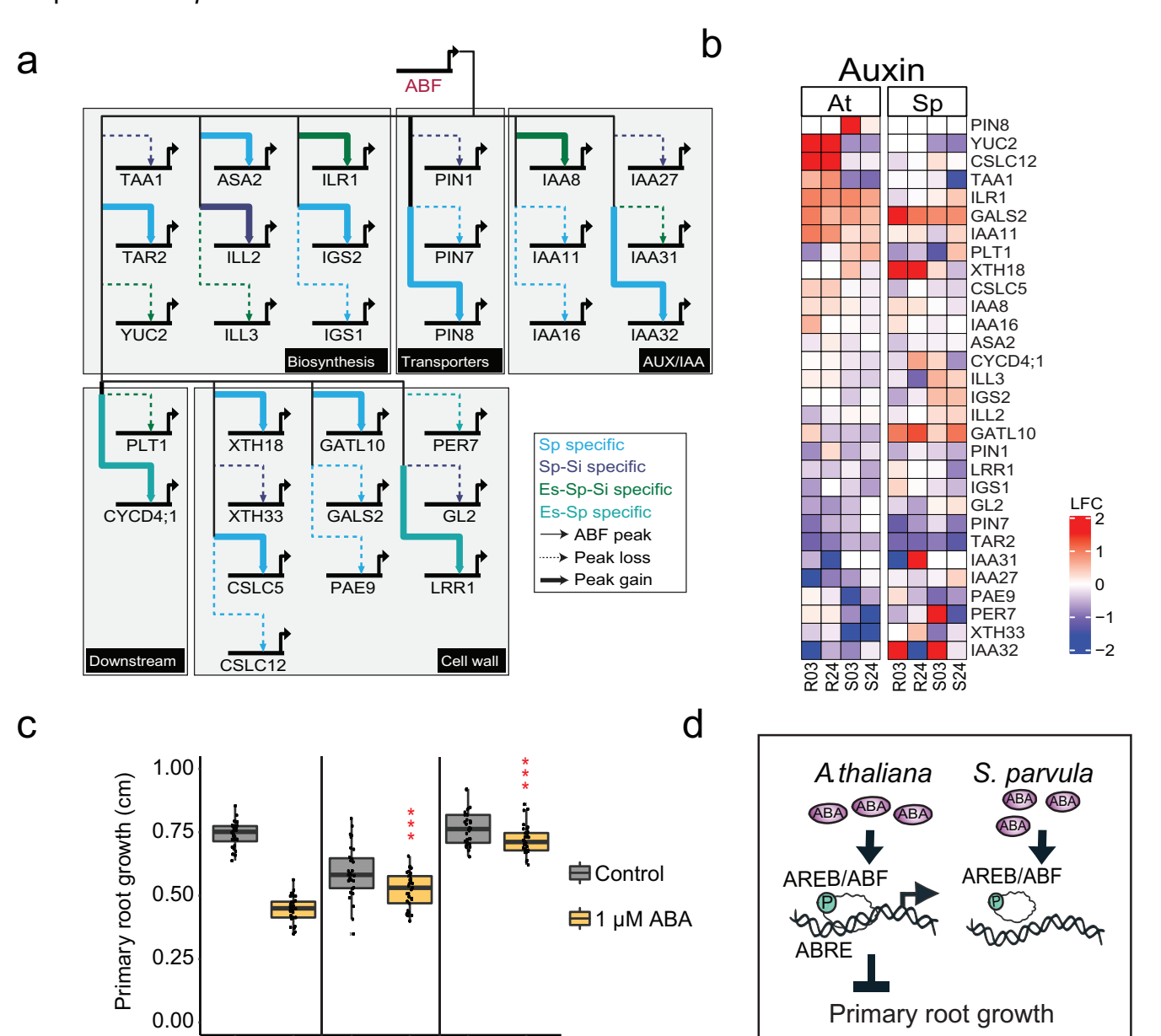


Figure 4: Rewiring of ABF-Auxin biosynthesis regulatory network is responsible for altered growth response in *S. parvula*.



WT+1 µM L-Kyn

WT

wei8-1